Experimental Investigations of Ground-Jet Suppression Fences for VTOL Aircraft Prepared Sites

K. H. Rogers,* R. Lavi,† and G. R. Hall‡
Northrop Norair, Hawthorne, Calif.

Small-scale and full-scale experiments show that a ground-jet suppression fence at the perimeter of a jet VTOL aircraft prepared pad is effective in reducing ground erosion and particle entrainment beyond the pad. The use of a small fence can reduce the required pad area by a factor of seven, for the same dynamic pressure (entrainment characteristics) near the ground beyond the pad. The fence is porous, with an inner ramp and an outer leg normal to the pad. The fence is located at about 15 equivalent jet nozzle diameters from the center of the jet impingement. A typical fence height for a hypothetical jet VTOL aircraft of 18,000-lb gross weight is 1.3 ft on a prepared pad of 47-ft radius. The fence has no effect on hot gas ingestion of the engines, and any sand or dust entrained beyond the fence remains in the confines of the ground-jet and is swept away radially.

Nomenclature

D	= diameter of single jet nozzle
D_e	= equivalent diameter of jet nozzles $D_e = Dn^{0.5}$ for n nozzles of D diameter each
H_f	= height of fence above ground plane
H_n	= height of jet nozzle exit above ground plane
P_n	= nozzle total pressure
P_s	= static pressure in ground-jet profile
P_T	= total pressure in ground-jet profile
P_∞	= ambient pressure (at infinity)
q	= dynamic pressure in ground-jet profile
q_{max}	= maximum dynamic pressure of ground-jet
$q_{0.5\ max}$	= one-half maximum dynamic pressure of ground-jet
R	= radial distance from jet nozzle centerline
R_f	= radial distance of fence from jet nozzle centerline
Re	= Reynolds number
T_{max}	= maximum temperature in ground-jet
T_n	= nozzle total temperature
T_∞	= ambient temperature (at infinity)
V	= velocity in ground-jet profile
X,Y	= ground reference axes
Z	= distance above ground plane (applicable to probe heights and positions in the ground-jet dynamic pressure profile)
$Z_{q\ max}$	= distance above ground plane of q_{max}
$Z_{0.5q\ max}$	= distance above ground plane of $0.5q_{max}$
α	= ramp angle of the fence
σ	= porosity of the fence = (open area/total area), the same for inner and outer legs of the fence, normal to plate surface

Introduction

A POTENTIALLY severe operational problem for jet-lift VTOL aircraft is the erosion of unprepared ground surfaces due to jet engine downwash during takeoff and landing. Development of various materials which can be spread over unprepared soil to form an erosion resistant VTOL pad has offered a solution to the erosion problem resulting from direct impingement of jet engine exhaust gases on the landing site.

An associated problem is the far-field entrainment of sand and debris resulting from the relatively high dynamic pressure of the ground-jet at some distance away from the landing site beyond the edge of the prepared pad. The natural decay of the ground-jet dynamic pressure to preclude particle entrainment beyond the edge of the pad results in a large and uneconomical pad size.

An approach to alleviate the entrainment problem is the use of a simple fence located around the periphery of the pad to reduce the ground-jet dynamic pressure, and thus permit reduction in pad diameter. In order to explore this solution to the entrainment problem, particularly for jet-lift VTOL aircraft, a program was undertaken to investigate the effectiveness of various fence geometries in suppressing the dynamic pressure of the ground-jet.

Objectives

The primary objectives of the program were to conduct small-scale and full-scale texts to identify fence configurations which are beneficial in reducing the ground-jet dynamic pressure downstream of the fence. The purpose of the small-scale investigation was to determine the effect of various fence configuration parameters and select suitable but fewer configurations for the full-scale tests. The purpose of the full-scale tests was to verify the results of the small-scale tests and to supply additional information in regard to the effect of fences on hot gas ingestion and the effect of configuration size (Reynolds number) on the ground-jet flow characteristics with and without fences.

Small-Scale Investigation

1. Selection of Small-Scale Fence Configurations

When a free jet impinges on a normal surface, a radially spreading ground-jet is produced. Such a flow is produced by the downward-directed exhaust gases from a VTOL aircraft. The ground-jet flowfield, which is essentially a viscous dominated flow composed of a free mixing region and a boundary layer, was first treated analytically[1] and later confirmed by experiments.[2]

Presented as Paper 68-639, at the AIAA 4th Propulsion Joint Specialist Conference, Cleveland, Ohio, June 10–14, 1968; submitted July 18, 1968; revision received January 13, 1969. The investigation was sponsored by the Air Force Aeropropulsion Laboratories, Wright-Patterson Air Force Base. Small-scale investigations were conducted at Northrop Norair; large-scale tests were made at the NASA Ames facility.

* Senior Technical Specialist, Research and Technology Department.

† Senior Scientist, Research and Technology Department. Associate Fellow.

‡ Member of Technical Management, Research and Technology Department. Associate Fellow.

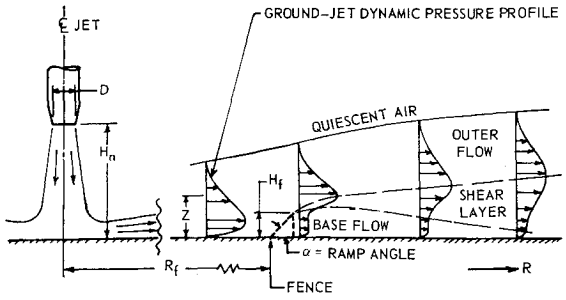

Fig. 1 Ground-jet flow with fence.

In the analysis[1] the entire ground-jet flow is assumed to be described by boundary-layer equations. For the case of a laminar ground-jet,[1] similar solutions for the velocity profiles (i.e., the nondimensional velocity distribution across the ground-jet does not vary with distance from the source) were obtained by integration of the governing boundary-layer equations. For the turbulent ground-jet, which is of more practical interest, the concept of an eddy viscosity was introduced and solutions for the boundary-layer and free mixing region were matched at the common interface. The results indicate that for high values of Reynolds number the thickness of the ground-jet increases approximately linearly with distance from the source, while the velocity decays at a rate approximately inversely with distance from the source.

Based on the natural velocity decay of the ground-jet,[1,2] along with ground erosion criteria,[3-5] the size of a prepared VTOL landing pad which would preclude erosion of the ground surface beyond the edges becomes excessive. The problem is to reduce the dynamic pressure of the ground-jet and reduce the size of landing-takeoff pad required, by means of a simple lightweight fence of reasonable dimensions while not aggravating other ground effect problems such as exhaust gas ingestion. In order to maintain reasonable dimensions, the fence must be effective while intercepting only the inner portion of the ground-jet. The function of the fence, then, is one of breaking up or deflecting the inner flow and providing separation of the outer flow from the ground plane.

The concept selected for investigating the above objective was a porous ramp configuration as shown in Fig. 1.

The ramp acts as a deflector in displacing the ground-jet away from the ground surface downstream of the fence while the porosity of the fence allows enough flow to pass through the fence to serve as a buffer layer between the higher energy outer flow and the ground plane, thereby reducing the strength of the vortex that occurs downstream of a solid fence, and reducing or eliminating the reverse flow near the ground resulting from such a vortex.

The test variables of the porous ramp configuration include the height of the fence relative to the thickness of the ground-jet, the porosity of the fence, and the ramp angle. Based on the preliminary analysis of fence effectiveness, the fence configurations listed in Table I were selected for evaluation in the small-scale tests. As indicated, tests were performed with both a single-nozzle and a dual-nozzle configuration in which the nozzle centerlines were spaced seven diameters apart. Nondimensional fence locations R_f/D were in the range 10 to 38.

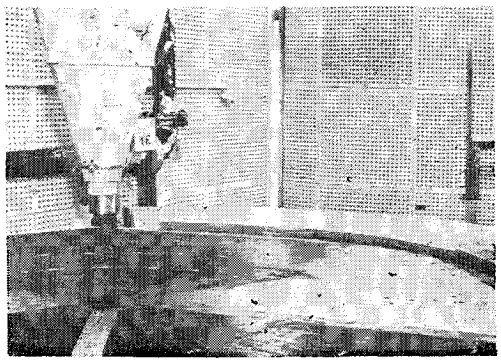

Fig. 2 Small-scale single-jet test setup.

Table 1 Parameters investigated

	Nozzle characteristics			
	Number of nozzles, n	Height ratio, H_n/D_e	Gas temperature, °R	
No fence	Single	5, 13.3	1050, 550	
	Dual	5	1050, 550	
	Fence characteristics			
	Number of nozzles, n	Height ratio, H_f/D_e	Angle α, deg	Porosity, σ
With fence	Single	0.33	30	0
		0.67	45	0.26
		1.00	60	0.42
				0.64
				0.70
	Dual	0.84	45	0
				0.42

2. Test Facility and Equipment

The small-scale test program was conducted in Northrop Norair's Inlet and Duct Test Facility. The test fixture for the small-scale single-jet (Fig. 2) tests consisted of a plenum discharging air through a 1.5-in.-diam nozzle. The air supply was provided by the high-pressure air system at ambient temperature for the cold flow test and at nominally 600°F for the tests at elevated temperatures. The nozzle directed the air jet vertically downward against a platform placed normal to the jet axis.

The test fixture for the dual-jet tests consisted of two vertical pipes with 1.25-in.-diam nozzles attached to the ends. The spacing between the nozzles was 7 nozzle diameters. The fence sections were mounted on the ground plane in a circular pattern at various distances from the nozzle centerline.

3. Instrumentation

A remotely positionable probe assembly, also called traveling rake, was used to survey the flowfield over the complete range of interest. The rake consisted of 12 total pressure probes, 6 static pressure probes, and 6 thermocouples to survey the flowfield ahead of and behind the fence. The rake measurements were made at intervals along a radial line from the single jet, and along a line from the centroid of impingement of the dual jets, normal to the common plane of the jets. The pressures were dispayed on water and/or slant alcohol manometer board and were photographically recorded. The temperatures were recorded on a multipoint Brown recorder. Plenum pressure and temperatures were similarly recorded.

4. Test Results and Discussion

The test results are concerned primarily with the effect of the various fence parameters in reducing the strength of the ground-jet dynamic pressure beyond the fence and near the ground surface. Figure 1 shows the geometric relationship of the nozzle, the dynamic pressure profile, and the fence, and shows the dimensional parameters investigated.

a. Ground-jet decay with no fence

The ground-jet decay with no fence was determined for a single jet at two different nozzle height ratios, $H_n/D = 5.0$

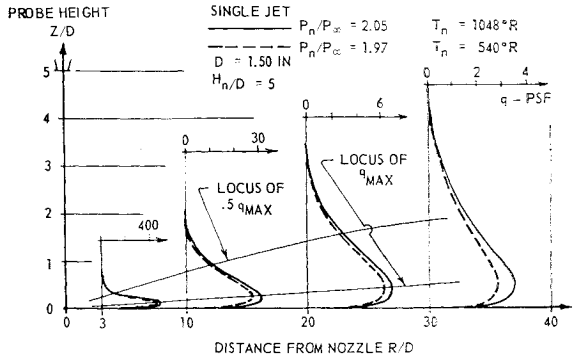

Fig. 3 Small-scale ground-jet dynamic pressure profiles with no fence.

and 13.3, and for dual jets at $H_n/D_e = 5.0$. All three combinations were tested with both hot and cold jets. Typical ground-jet dynamic pressure profiles are shown in Fig. 3, for the single jet.

The ground-jet thickness from the single jet increases almost linearly with the distance from the nozzle centerline. The ground-jet dynamic pressure profiles in the interaction plane from the dual nozzles are appreciably thicker than those of the single nozzle. The decay of the maximum dynamic pressure of the ground-jet for all of the no-fence tests is shown in Fig. 4. The results show that a pad radius in the order of 40 equivalent nozzle diameters is required to reduce the ground-jet dynamic pressure below 2 psf. The decay of dynamic pressure, nondimensionalized, is compared with corresponding full-scale data in the discussion of the full-scale test results. Temperature measurements show a higher temperature of the ground-jet for the dual-nozzle configuration. The temperature decay data, nondimensionalized, are compared with full-scale data in the discussion of the full-scale test results.

b. Ground-jet dynamic pressure profiles beyond the fence

All of the fence configurations tested, except the lowest fence, reduced the dynamic pressure to values less than 2 psf near the ground beyond the fence. The dynamic pressure profiles beyond the fence are shown for three selected test configurations (Figs. 5–7). All apply to fences with face or ramp angle $\alpha = 45°$, with the fence located at different radial distances from the nozzle centerline.

The principal parameters compared in the three figures are shown in Table 2.

In the figures showing dynamic pressure profiles of the ground-jet, the Z scale (height) is expanded relative to the X scale (ground distance) in order to clearly show the ground-jet profile near the ground. Consequently, the cross section of the fence appears distorted (too slender) in the figures.

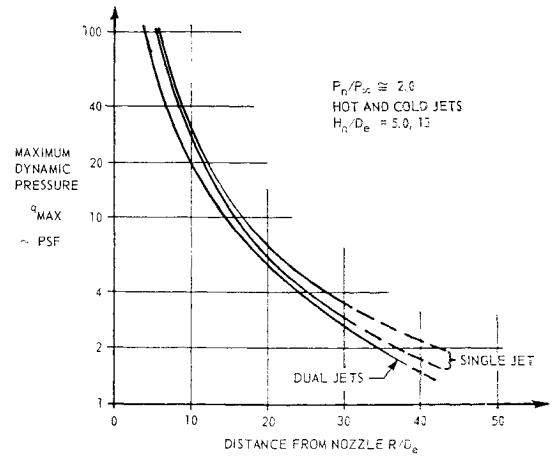

Fig. 4 Small-scale ground-jet decay of maximum dynamic pressure with no fence.

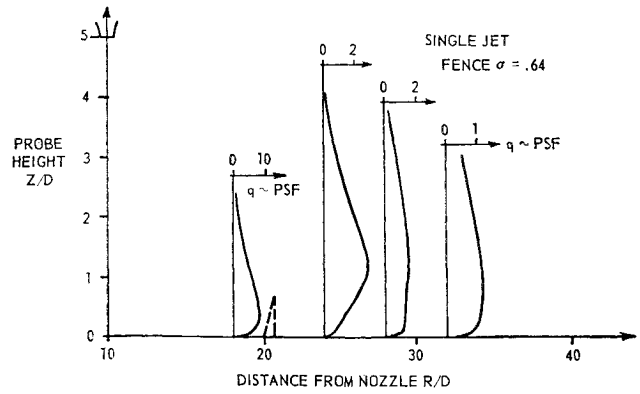

Fig. 5 Small-scale ground-jet dynamic pressure profiles with high porosity fence.

Figures 5–7 show three types of flow due to the fence. For a highly porous fence (Fig. 5), the ground-jet may remain attached to the ground through and beyond the fence. A less porous or solid fence may cause the flow to separate at or near the fence and reattach at a relatively short distance beyond the fence, creating a standing vortex on the downstream side of the fence (Fig. 6). But if the fence height is large compared with the height of the bulge of the ground-jet dynamic pressure profile, as in the case of the highest fence at the nearest radial location, the ground-jet may be deflected upward by the fence and may behave similarly to a free jet without reattachment to the platform beyond the fence (Fig. 7). Flow characteristics from the dual jets are similar to those described for the single jet.

c. Reduction in dynamic pressure due to fence

The reduction in dynamic pressure due to the fence can be shown effectively by superposing the results on a plot of dynamic pressure decay with no fence. An example, applicable to the single jet, is shown in Fig. 8. The maximum dynamic pressure and the dynamic pressure 0.3 in. above the surface are shown. Figure 8 is typical for separated flow with reattachment, for a fence only 10 diameters from the nozzle centerline. To show the effect of the fence in reducing the dynamic pressure of the ground-jet, it is convenient to consider two pads of the same diameter, one with a fence and one without a fence. Again referring to Fig. 8, the maximum dynamic pressure beyond the pad is reduced greatly by the fence, and the dynamic pressure at a height of 0.3 in. increases from zero after reattachment. Apparently both are approaching a value near 1.3 psf a short distance

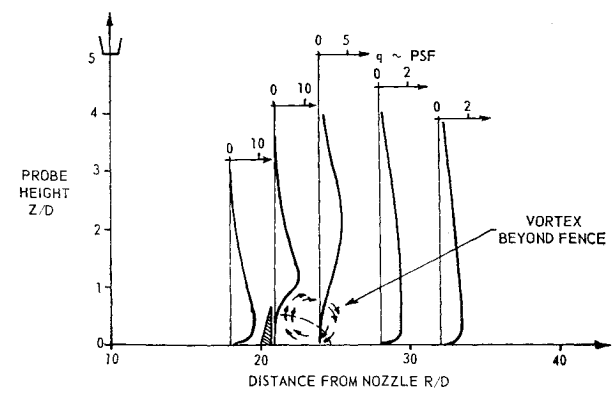

Fig. 6 Small-scale ground-jet dynamic pressure profiles with solid fence.

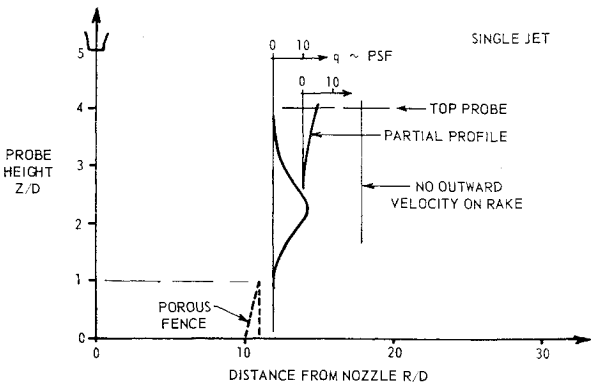

Fig. 7 Small-scale ground-jet dynamic pressure profiles with high fence at $R_f/D = 10$.

beyond the fence, as compared with a pressure of about 20 psf at the edge of the pad for the no-fence configuration.

In the preceding example, and in other test results not shown, the dynamic pressure beyond the prepared pad was reduced by factors of roughly 20, 10, and 6 for fence distances of 10, 15, and 20 effective diameters, respectively. The corresponding reduced values of dynamic pressure near the ground (0.3 in. above the ground) ranged from 1.3 to 0.8 psf. Experimental data[3] indicate that the threshold for entrainment of dry loose dirt and dry fine sand is a dynamic pressure of slightly more than unity near the ground.

In addition to the rake readings, which measured dynamic pressure in the outward direction only, a limited survey of velocities in the reverse flow or vortex region just beyond the fence was made with a hot wire anemometer for several fence configurations. The results show that the reverse flow in the vortex near the surface often is comparable in magnitude to the outward velocity after reattachment of the separated flow. A typical maximum value of reverse flow dynamic pressure measured at a height of about 0.15 in. was 0.4 psf. A detailed determination of reverse flow profiles in the vortex region was beyond the scope of the investigation.

d. Selection of full-scale fence parameters

An examination of the small-scale test results shows that the fence height ratio H_f/D_e and the fence radius ratio R_f/D_e are of primary importance to the reduction of dynamic pressure near the ground beyond the fence, and the fence inner face or ramp angle α and fence porosity σ are of secondary importance. The effect of these four parameters on full-scale fence selection is discussed in the following paragraphs.

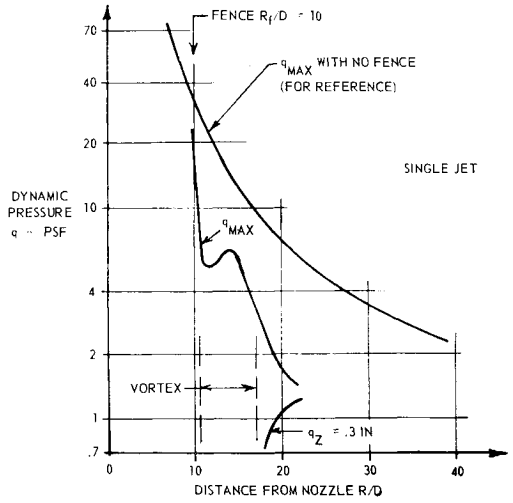

Fig. 8 Dynamic pressure reduction due to fence—small scale.

Table 2 Principal parameters

Figure no.	Fence parameters: Number of jets	Height ratio H_f/D_e	Porosity
5	1	0.67	0.64
6	1	0.67	0.42
7	1	1.00	0.42

The dynamic pressure of the reattached flow, 0.3 in. above the ground, is shown in Fig. 9 as a function of the fence height and fence radius. The plot applies to average values of fence angle and porosity investigated. The practical aspects of fence application to a prepared site for a research VTOL aircraft (Fig. 10) may require a fence radius ratio R_f/D_e equal to 15–20. Another consideration in the fence selection is the criterion that the dynamic pressure near the ground should be less than 1.5 to avoid entrainment of any particles larger than fine sand or dust, and less than unity to avoid entrainment of fine sand or dust. These criteria are based on experimental data.[3] Returning to Fig. 9, in the band of fence radius ratios 15–20, and dynamic pressure less than 1.5 psf, the fence height ratio must be greater than 0.50. A maximum fence height ratio of 1.3 is required for reattachment on the platform beyond the fence. The full-scale engine combinations provide equivalent engine nozzle diameters of 1.05 ft, 1.485 ft, and 1.82 ft. The selected full-scale fence height was 1.25 ft, which resulted in fence height ratios within the optimum band of 0.50 to 1.3 for all three engine combinations, neglecting Reynolds number effects. The minimum full-scale fence radius selected was 18.2 ft, resulting in a minimum fence radius ratio of 10.

The dynamic pressure near the ground beyond the fence was plotted vs radial distance for ramp angles of 30°, 45°, and 60°, for several different combinations of fence height and porosity. The results in every case show that the 45° fence is most effective on the basis of lowest dynamic pressure beyond the fence. Therefore, a 45° face angle (ramp angle) was selected for the full-scale tests.

Test results similar to those described in the preceding paragraph show that the medium porosity $\sigma = 0.42$, is best. The high porosity fence allows excessive flow-through, resulting in relatively high dynamic pressures immediately beyond the fence. The zero porosity or solid fence on the other hand creates a stronger vortex configuration beyond the fence. Thus, a porosity of 0.42 was selected for the full-scale tests.

Full-Scale Investigation

1. Test Facility and Equipment

The full-scale tests were conducted at the NASA Ames Research Center Static Test Facility. This facility is an

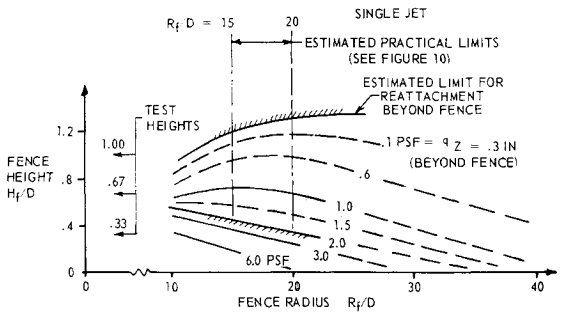

Fig. 9 Dynamic pressure near ground as a function of fence height and radius—small scale.

Table 3 Full-scale test configurations

Fence		Engine	
Distance, R_f = ft	Porosity, σ	Combinations	Nozzle height, $H_n \sim$ ft
No fence,		All	
X axis		3, 2–4, 2–3–4	5.25, 9.45
36.4	0, 0.42		5.25
X axis			
27.3	0, 0.42		5.25, 9.45
X axis			
18.2	0.42		5.25, 9.45
X axis			

outdoor complex design to support powered models and aircraft in hover tests at varying heights above ground and different angles of attack (Fig. 11).

2. VTOL Model

The VTOL model (Fig. 11) consisted of four General Electric YJ85 engines without afterburners mounted vertically in the center fuselage on 30.5 in. centers. A maximum of three engines (engines 2–4) were operated during the test program.

3. Ground-Jet Suppression Fences

Figure 11 also shows one of the ground-jet test fences mounted at the mid-distance (R_f = 27.3 ft) of the three fence locations tested. The fences were 1.25 ft high, with ramp angle α = 45° and outer face normal to the ground plane. Two fence porosities were tested at each location; σ = 0 (solid) and σ = 0.41. Each fence section was five feet long and formed from a single sheet of 0.05 steel; thus, the porosity and thickness of inner and outer face were equal. The fences were tested on the east or left side of the model.

4. Test Configurations

The line extending east or left from engine number three (X axis) is the center-line locus of the fence and rake positions beyond the fence. All of the fence tests were made on the X axis. The ground-jet rakes are shown in Fig. 11 and are described in Instrumentation. All three engine combinations, 3, 2–4, and 2–3–4, were tested in each of four planform configurations. The different planforms varied in rake location and fence location. Table 3 shows the configurations tested.

The ground-jet rake measurements were supplemented with sand entrainment tests. The first sand entrainment test was made with no fence, three engines, and coarse sand (16 mesh) only. The next four sand entrainment tests were made with porous and solid fences at 36.4 ft, with single as well as with three engines operating. Both fine sand (30 mesh) and coarse sand were used. Most of the fine sand particles were in the size range 0.01- to 0.03-in. diam. Most of the coarse sand particles were in the size range 0.04- to 0.08-in. diam. The final four tests of sand entrainment were like the preceding four except that the fences were moved to the midposition (R_f = 27.3 ft).

5. Instrumentation

Full-scale test instrumentation was designed to define the ground-jet and measure the pertinent engine performance parameters. Five rakes were employed to investigate the ground-jet. Three of the rakes consisted of 11 total pressure, 7 static pressure probes, and 6 thermocouples. The other two rakes were similar except no thermocouples were employed.

Table 4 Engine nozzle pressure ratio and temperature

	Nozzle, pressure ratio, $P_n/P\infty$	Nozzle temperature, $T_n \sim$ °R
Fullscale	1.7	1450
Smallscale	2.0	1050

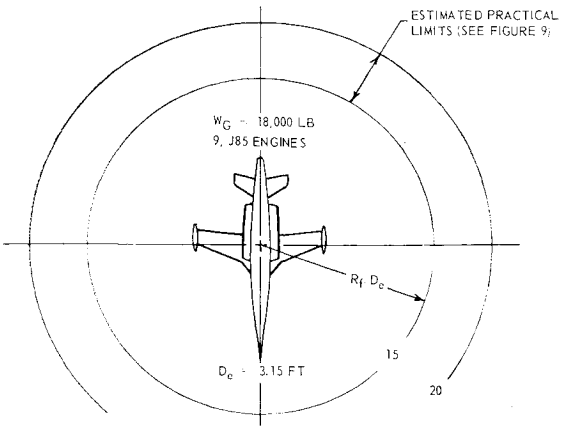

Fig. 10 Hypothetical VTOL research airplane on VTOL pad.

6. Test Results and Discussion

The full-scale tests are divided into two groups: the no-fence tests and the fence tests. The no-fence tests determine the basic ground-jet flow characteristics for three different engine combinations and two different nozzle heights above the ground plane. The fence tests determine the reduction in the dynamic pressure of the ground-jet near the ground beyond the fence for three different fence locations and for solid and porous fences. These tests are supplemented by investigations of the effect of fences on the reingestion of hot gases and by motion pictures of sand entrainment. The engine nozzle pressure ratio and temperature are similar to but not the same as those of the small-scale tests. Representative values are shown in Table 4.

a. No-fence tests

1) Ground-Jet Dynamic Pressure Profiles—No Fence: the full-scale ground-jet dynamic pressure profiles with no fence are very similar in shape to those of the small-scale tests.

2) Decay of Ground-Jet Maximum Dynamic Pressure—No Fence: the reduction in the maximum dynamic pressure ratio of the ground-jet with distance from nozzle is shown in Figs. 12 and 13 for the single-engine and dual-engine tests, respectively. The results for the three-engine configuration are comparable to those presented for the dual engine tests.

The results are presented in a nondimensional form, referenced to the difference between nozzle and ambient pressures, and are compared with results from the small-scale tests. The multiengine full-scale results show a leveling off and apparent increase in maximum dynamic presure with distance in the far field (about 30 equivalent diameters from the engines). The reason for this phenomenon is not completely known.

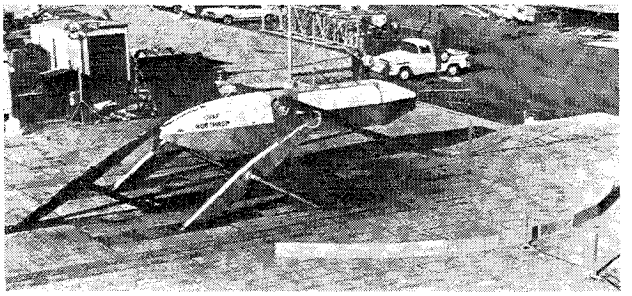

Fig. 11 Full-scale test setup with engine bays enclosed.

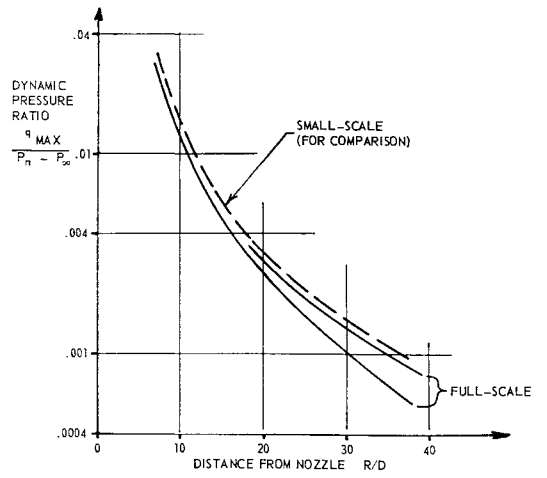

Fig. 12 Ground-jet decay of maximum dynamic pressure ratio—single jet no fence.

3) Ground-Jet Temperature Decay—No Fence: Fig. 14 shows the reduction in ground-jet temperature with distance from the nozzle centerline for the different engine combinations with no fence. Small-scale results are shown in dashed lines for comparison. The temperature parameter is the difference between ground-jet maximum temperature and ambient temperature, divided by the difference in nozzle and ambient temperatures. The temperature of the full-scale ground-jet appears to be a smaller fraction of the source temperature than does that of the small-scale ground-jet.

4) Ground-Jet Thickness—No Fence: the curves of ground-jet height at q_{max} for the single-engine configuration are grouped together and compared with small-scale test results in Fig. 15. Similar results apply to the dual-engine tests. The results show that the full-scale ground-jet height at q_{max}, nondimensionalized with respect to nozzle equivalent diameter, is appreciably less than that of the small-scale tests, at distances corresponding to full-scale fence test locations. The difference is a Reynolds number effect associated with the growth of the turbulent boundary layer.

b. Fence tests

1) Ground-Jet Dynamic Pressure with Fence: in general, the ground-jet dynamic pressure profiles measured beyond the fence in the full-scale investigation confirm the results of the small-scale tests. All three flow configurations shown in Figs. 5–7 were repeated in the full-scale tests. The main difference in the full-scale fence tests was that the fence was higher relative to the height of the ground-jet, resulting in larger vortex formations beyond the fence for most of the configurations. The reverse flow in the vortex was measured only indirectly, by sand entrainment. The sand entrainment tests clearly show that the vortices beyond the porous fence are weaker than those beyond the solid fence. For example, at the fence middle distance of 27.3 ft with three engines operating, only fine sand is entrained by the vortex beyond the porous fence, but both fine and coarse sand are entrained by the vortex beyond the solid fence. The dynamic pressure profiles for the former test, showing a rather extensive vortex beyond the fence, are plotted in Fig. 16. Perhaps a weaker vortex and less sand entrainment would result from a smaller fence.

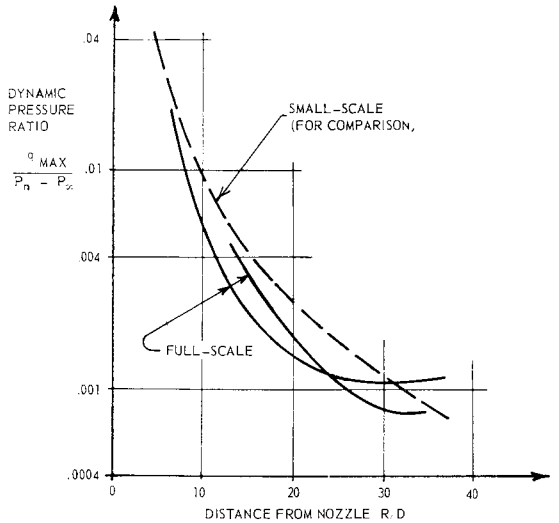

Fig. 13 Ground-jet decay of maximum dynamic pressure ratio—dual jets no fence.

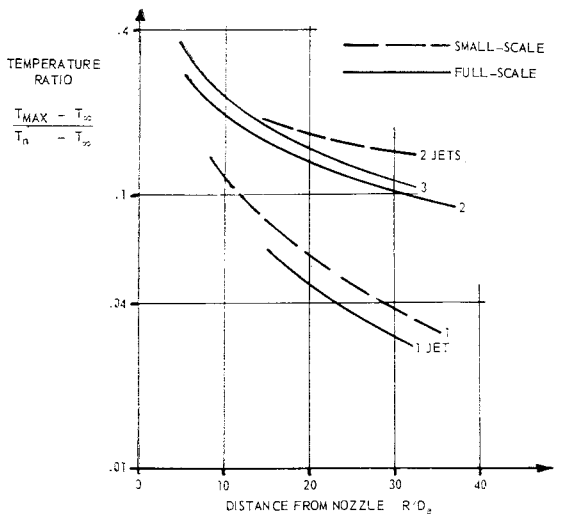

Fig. 14 Ground-jet temperature ratio decay—no fence.

2) Effect of Fences on Hot Gas Ingestion at Engine Inlets: the fences appear to have no effect on engine inlet temperatures.

3) Sand Ingestion Due to Sand Entrainment Beyond the Fence: in the sand entrainment tests, some sand is circulated in the vortex region, some piled in a ring beyond and near the fence, and some is carried away radially within the height of the ground-jet profile. Apparently none of it recirculates into the inner region bounded by the fence.

Conclusions

1) A VTOL pad radius of about 15 equivalent jet nozzle diameters appears to be adequate if a porous fence is mounted on the periphery of the pad. On the other hand, to achieve comparable values of ground-jet dynamic pressure near the ground beyond a no-fence pad, the required pad radius is about 40 equivalent jet nozzle diameters. Thus, the use of a

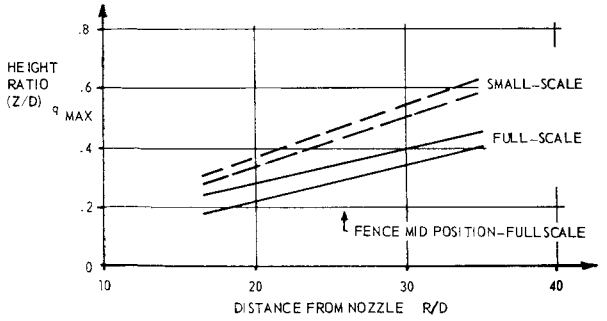

Fig. 15 Height of ground-jet maximum dynamic pressure—no fence.

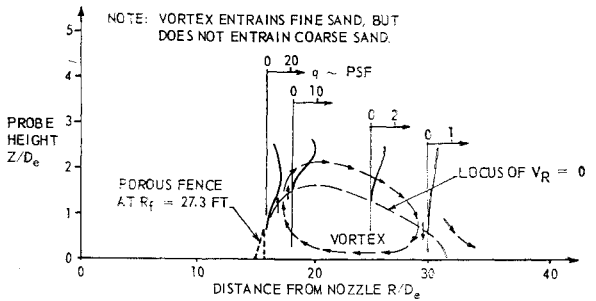

Fig. 16 Full-scale ground-jet dynamic pressure profiles with porous fence at $R_f = 27.3$ ft and three jet engines at $H_n = 5.25$ ft.

porous fence reduces the required pad area by a factor of $(40/15)^2 \cong 7$.

2) A porous fence is more effective than a solid fence in reducing the dynamic pressure of the ground-jet beyond the fence without creating a vortex of appreciable strength. A fence porosity of 42% and a fence ramp angle of 45° appear to be near-optimum values.

3) The required fence height is closely related to the height of the ground-jet, and also to the ramp angle and porosity of the fence. The optimum height of the porous fence, based on small-scale test results at a distance of 15 equivalent jet nozzle diameters, and corrected for Reynolds number effect (size effect) based on full-scale tests, can be expressed approximately as $H_f = 0.10(D_e/0.125)^{0.8}$ ft.

4) The elimination of sand or dirt entrainment beyond a porous fence located at 15 equivalent jet nozzle diameters from the centroid of jet impingement appears to be possible, on the basis of small-scale test results. Fine sand was entained in this configuration in the full-scale tests, but the fence height may not have been optimum. The entrained sand was carried away radially within the ground-jet and did not recirculate within the pad area.

5) The ground-jet suppression fences have no noticeable effect on the hot gas ingestion characteristics of the engines.

References

[1] Glauert, M. B., "The Wall Jet," *Journal of Fluid Mechanics*, Vol. 1, Aug. 1956, p. 625.

[2] Bakke, P., "An Experimental Investigation of a Wall Jet," *Journal of Fluid Mechanics*, Vol. 2, July 1957, p. 467.

[3] Kuhn, R. E., "An Investigation to Determine Conditions under Which Downwash from VTOL Aircraft Will Start Surface Erosion from Various Types of Terrain," TN D-56, Sept. 1959, NASA.

[4] Vidal, R. J., "Aerodynamic Processes in the Downwash Impingement Problem," Paper 62-36, Jan. 1962, IAS.

[5] Harris, A. W., Marbest, J. A., and Tatom, J. W., "VTOL Transport Exhaust Gas Ingestion Model Tests," Paper 17, 7th Annual National Conference on Environmental Effects on Aircraft and Propulsion Systems, Princeton, N. J., Sept. 1967.